NANO LETTERS

Letter

pubs.acs.org/NanoLett

van der Waals Epitaxy of MoS_2 Layers Using Graphene As Growth Templates

Yumeng Shi,[†,‡,#] Wu Zhou,[∥,⊥,#] Ang-Yu Lu,[§] Wenjing Fang,[†] Yi-Hsien Lee,[§,†] Allen Long Hsu,[†] Soo Min Kim,[†] Ki Kang Kim,[†] Hui Ying Yang,[‡] Lain-Jong Li,[§] Juan-Carlos Idrobo,[⊥] and Jing Kong*[,†]

[†]Department of Electrical Engineering and Computer Sciences, Massachusetts Institute of Technology, Cambridge, Massachusetts 02139, United States

[‡]Singapore University of Technology and Design, 20 Dover Drive Singapore 138682, Singapore

[§]Institute of Atomic and Molecular Sciences, Academia Sinica, Taipei, 11529, Taiwan

[∥]Department of Physics and Astronomy, Vanderbilt University, Nashville, Tennessee 37235, United States

[⊥]Materials Science and Technology Division, Oak Ridge National Laboratory, Oak Ridge Tennessee 37831-6064, United States

S *Supporting Information*

ABSTRACT: We present a method for synthesizing MoS_2/Graphene hybrid heterostructures with a growth template of graphene-covered Cu foil. Compared to other recent reports,[1,2] a much lower growth temperature of 400 °C is required for this procedure. The chemical vapor deposition of MoS_2 on the graphene surface gives rise to single crystalline hexagonal flakes with a typical lateral size ranging from several hundred nanometers to several micrometers. The precursor (ammonium thiomolybdate) together with solvent was transported to graphene surface by a carrier gas at room temperature, which was then followed by post annealing. At an elevated temperature, the precursor self-assembles to form MoS_2 flakes epitaxially on the graphene surface via thermal decomposition. With higher amount of precursor delivered onto the graphene surface, a continuous MoS_2 film on graphene can be obtained. This simple chemical vapor deposition method provides a unique approach for the synthesis of graphene heterostructures and surface functionalization of graphene. The synthesized two-dimensional MoS_2/Graphene hybrids possess great potential toward the development of new optical and electronic devices as well as a wide variety of newly synthesizable compounds for catalysts.

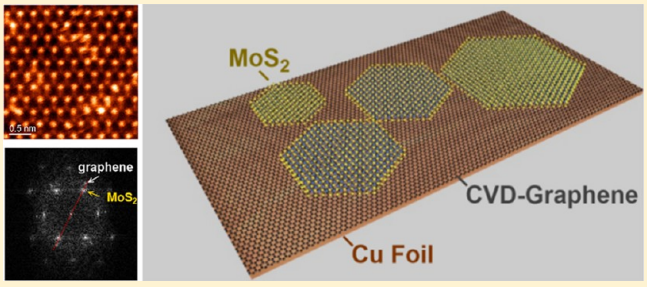

KEYWORDS: *Chemical vapor deposition, van der Waals epitaxy, molybdenum disulfide, graphene, STEM imaging*

Atomically thin two-dimensional (2D) materials with a layered structure such as graphene[3−5] and hexagonal boron nitride (h-BN)[6,7] have been attracting a large amount of attention due to their unique properties.[4,8−10] Recently, it has been demonstrated that molybdenum disulfide (MoS_2), another inorganic graphene analogue, exhibits excellent electrical[11] and optical performance[12,13] when it is thinned down to a monolayer. MoS_2 belongs to the layered transition-metal dichalcogenides (LTMDs) materials, which are traditionally used as solid-state lubricants and as catalysts for hydrodesulfurization and hydrogen evolution. Similar to graphene and h-BN, MoS_2 has a hexagonal crystal structure.[14] Each Mo atom is six-fold coordinated, hexagonally packed between two three-fold coordinated sulfur atoms. Each S−Mo−S quintuple-layer is weakly boned to other S−Mo−S layers by van der Waals forces.

Because of the relatively weak interaction between the S−Mo−S layers, physical[11,15] or chemical exfoliation[16,17] methods can be used to cleave the MoS_2 flakes down to ultrathin crystals typically with thicknesses of ∼0.65 nm. It has been reported that the electrical and optical properties of MoS_2 change dramatically from bulk MoS_2 to monolayer (i.e., a S−Mo−S quintuple layer) due to the interlayer interaction.[15] Bulk MoS_2 is a semiconducting material with an indirect band gap of ∼1.2 eV, while monolayer MoS_2 is a direct band gap material with a band gap of ∼1.8 eV.[17] Recently, monolayer MoS_2 field effect transistors (FETs) have been fabricated.[11] By using halfnium oxide (HfO_2) as the gate dielectric, electron mobility up to 200 $cm^2\ V^{-1}\ s^{-1}$ with an on/off current ratio of more than 10^8 has been achieved.[11] However, unlike graphene that does not have a band gap, MoS_2 presents a band gap, and that makes it a more attractive material for optoelectronics[18] and low power digital electronics.

Besides the top down exfoliation method, MoS_2 can be synthesized using different bottom up approaches, such as transition metal sulfurization,[1,19−22] thermal decomposition of

Received: December 28, 2011
Revised: May 19, 2012
Published: May 29, 2012

   dx.doi.org/10.1021/nl204562j | *Nano Lett.* 2012, 12, 2784−2791

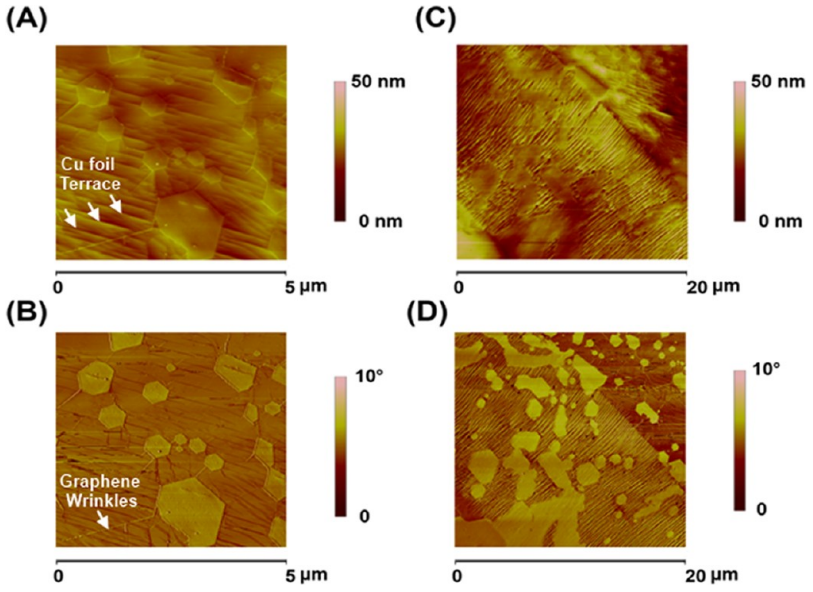

Figure 1. MoS_2 nanoflakes on CVD graphene/Cu foil substrates. (A,C) Typical AFM height images of MoS_2 flakes grown on graphene/Cu foil substrates. (B,D) AFM phase images of the corresponding regions as shown in A and C. For these samples, the precursor adsorption time was 10 min with Ar flow rate of 10 sccm as the precursor carrying gas.

thiosalts,[2,23−25] vapor transportation,[26,27] and solvothermalization.[28−30] Recently, chemical vapor deposition (CVD) has been successfully used to synthesize large area high quality 2D materials such as graphene[31−33] and boron nitride[34−36] on transition metals. Compared to other synthesis methods, CVD potentially can give better control over the number of layers if the growth occurs via surface mediated synthesis. Especially for a material like MoS_2, where the band gap varies from the bulk down to monolayer, it is desirable to achieve atomic layer control over the number of MoS_2 layers synthesized. Most recently, large-area MoS_2 atomic thin layers have been obtained by either sulfurization of thin molybdenum layers[1] or thermal decomposition of ammonium thiomolybdate in a sulfur rich environment.[2] Both of these methods include high-temperature annealing process over 800 °C.

Apart from the effort of achieving mono- or few-layer MoS_2, progress has also been made in the growth of hybrid graphene/MoS_2 structures. It has been demonstrated that reduced graphene oxide (RGO) can be a good template for MoS_2 nanoflakes formation[37] by simply dissolving ammonium thiomolybdate ($(NH_4)_2MoS_4$) together with RGO in an organic solvent at an elevated temperature. The heterostructures of graphene/MoS_2 hybrids show great potential in the hydrogen evolution reaction (HER).[37] Furthermore, these graphene/MoS_2 hybrids are not just limited to catalysis applications, they are also model systems to study the physics of interfaces between two-dimensional layers, or even p−n junctions at these interfaces, and this also opens a new way for graphene functionalization. However, due to the defective nature of RGO the solvothermal method only produces small crystallites of MoS_2 (lateral size ∼2 nm).[37]

Previously, it has been demonstrated that graphite can be a good template for bilayer Bernal-stacked graphene[38] and the growth of topological insulators[39] via van der Waals epitaxy. An essence of the van der Waals epitaxy is to obtain a substrate surface that is free of dangling bonds.[40,41] The graphene surface, formed by sp^2 bonded carbon atoms, is atomically flat and free of dangling bonds, which makes it an ideal starting template for other 2D materials. In this work, we introduce a method for synthesizing high quality MoS_2 single crystal flakes (with lateral sizes up to several micrometers) on a CVD grown graphene (CVD-G) surface. Compared to the most recently reported methods,[1,2] we demonstrate MoS_2 nanoflakes can be epitaxially synthesized on the surface of graphene at relatively low temperature of 400 °C. The relatively large lattice mismatch between MoS_2 and graphene (∼28%)[42] is expected to be relaxed through the week van der Waals force. Compared to the conventional van der Waals epitaxy, we use organic solvent to carry and deposit the precursor onto the surface of CVD-G. After postannealing, the MoS_2 layers form on the surface of graphene with their *c*-axis perpendicular to the graphene surface. It is believed that the interface properties of CVD-G, that is, free of dangling bonds and intrinsic weak van der Waals forces play an important role in the MoS_2 growth. Yet, a precise control on the number of layers for the growth of MoS_2 on graphene surface is still not achieved. For instance, at a low dose of $(NH_4)_2MoS_4$ precursor, isolated MoS_2 thin flakes form on the surface of graphene and an increment of the precursor dose produces thicker MoS_2 flakes, which eventually results in a continuous MoS_2 film on the graphene surface. Nevertheless, the obtained MoS_2 nanoflakes in this study possess high crystallinity and have abundant edges, which can be very useful in applications such as catalysis,[37,43,44] sensing,[45] or energy storage,[46−48] where the thickness control of MoS_2 is less critical. The MoS_2/graphene heterostructure was evaluated by atomic force microscopy (AFM), transmission electron microscopy (TEM), X-ray energy dispersive spectrometer (EDS) spectrum, aberration-corrected scanning transmission electron microscopy (STEM), electron energy loss spectroscopy (EELS), Raman spectroscopy, and X-ray photoelectron spectroscopy (XPS).

Results and Discussion. The MoS_2/CVD-G hybrid was obtained in a low-pressure chemical vapor deposition (LPCVD) system. The precursor for MoS_2 growth is $(NH_4)_2MoS_4$, which is a solid at room temperature. In order to deposit the precursor in a controllable manner, $(NH_4)_2MoS_4$

dx.doi.org/10.1021/nl204562j | *Nano Lett.* 2012, 12, 2784−2791

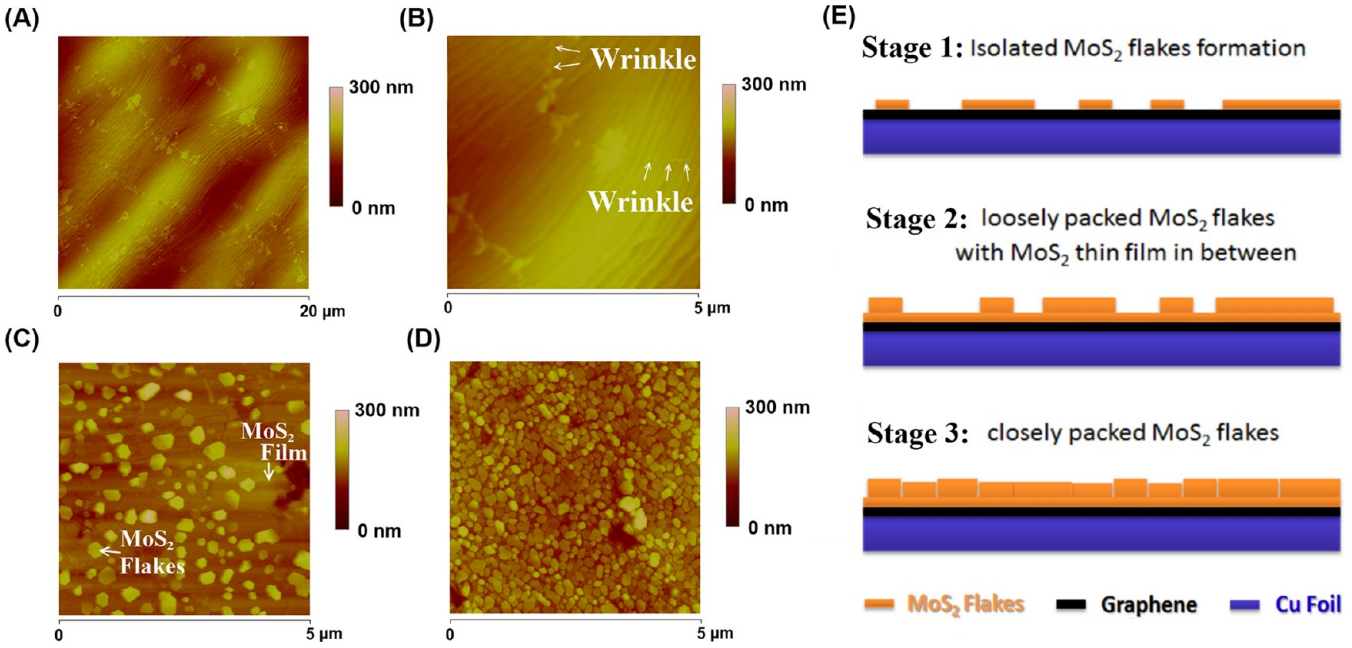

Figure 2. AFM images showing the formation of nanoflakes under different growth conditions. (A,B) AFM images of the sample surface after growth with very low amount of precursor supply, showing formation of small flakes along the graphene wrinkles at the initial stage of precursor adsorption. (C,D) AFM images of the sample surface after growth with high amount of precursor supply (precursor adsorption time was 30 min and 1 h for panels C and D, respectively). Hexagonal-shaped nanoflakes were found fully covering the surface after 1 h of growth. (E) Schematic diagram showing the formation of MoS_2 flakes and thin films under different growth conditions. On stage 1, the amount of precursor is limited, which gives isolated MoS_2 flakes. With increasing amount of precursor, the surface coverage of MoS_2 flakes increases with thin MoS_2 films forming in between the flakes. On stage 3, the amount of precursor further increases which results in closely packed MoS_2 nanoflakes on the MoS_2 film.

is dissolved in *N*,*N*-dimethylformamide (DMF), and by bubbling the organic solution with argon (Ar) gas the DMF/$(NH_4)_2MoS_4$ vapor can be carried into the growth chamber and subsequently adsorbed onto the surface of the CVD-G. The amount of precursor deposition can be adjusted by varying the flow rate of the carrying gas, the concentration of the DMF/$(NH_4)_2MoS_4$, and the deposition time. After exposing the CVD-G to the precursor, the growth chamber was heated up to 400 °C at a heating rate of 5 °C/min. At the growth temperature, the precursor fully decomposes into MoS_2 and generates S, H_2S, and NH_3 gas. More details of the growth condition are described in the Supporting Information.

The as-grown MoS_2/graphene heterostructures were identified by AFM. Figure 1A,B shows the height and phase images (taken in tapping mode AFM) of the MoS_2 flakes grown on a single layer CVD-G substrate. The precursor adsorption time was 10 min with Ar flow rate of 10 standard cubic centimeters per minute (sccm) as the precursor carrying gas. The location of the MoS_2 flakes can be more easily identified by the phase image (as shown in Figure 1B,D). The MoS_2 flakes tend to have a hexagonal or quasi-hexagonal shape (with a lateral size ranging from several hundred nanometers to several micrometers and a typical thickness from ~2 to ~5 nm) with a higher phase color contrast compared to graphene on Cu foil. It was also found that when graphene oxide or bare Cu foil is used as growth template there is no hexagonal shape MoS_2 flakes that can be obtained, which suggests the growth of MoS_2 can be affected considerably by the crystal quality of graphene underneath. Figure 1C,D shows the AFM phase image of the MoS_2 grown on graphene over 20 μm × 20 μm region. As indicated in Figure 1A, for the as-grown samples terrace structure from Cu foil surface can be frequently observed and the synthesized MoS_2 flakes are found to cross these Cu foil terraces. However, there appears to be no correlation between the location of the MoS_2 flakes and the Cu terraces. These observations suggest the CVD-G interlayer plays an important role on the MoS_2 growth.

Meanwhile, as seen in Figure 1A, graphene wrinkles normally can be found around the MoS_2 flakes. From our previous report, the graphene wrinkles are more reactive than the surface plan region,[49] which could attract the precursor at the initial stage and act as the first nucleation center for MoS_2 growth. To verify this, the nucleation of the MoS_2 on the graphene surface was investigated by limiting the amount of precursor during the adsorption step. For this purpose, the adsorption time was fixed at 10 min with Ar flow rate of 10 sccm as the precursor carrying gas, but this Ar-carried DMF/$(NH_4)_2MoS_4$ vapor was diluted by another 100 sccm Ar gas before reaching the deposition zone. Figure 2A shows the AFM images of the MoS_2 growth with an extremely small amount of precursor adsorption. For the CVD grown graphene on metal, normally wrinkles form due to the negative thermal expansion coefficient of graphene. It was found that after the growth, the wrinkled regions tend to have more MoS_2 flakelike features (as indicated in Figure 2B) and those features follow the wrinkles very well. This phenomenon suggests the graphene wrinkles can effectively serve as the first nucleation centers. With an increased amount of precursor, the MoS_2 can grow on the surface of graphene through weak van der Waals interaction. The nucleation of MoS_2 on the graphene wrinkles is probably due to the curved sp^2 π bonds in the graphene wrinkles, which have been shown to be more reactive than the planar graphene regions.[49] A recent report shows that the dangling bonds at the graphene boundaries are likely to attract adsorbates.[50] Therefore, the grain boundaries of CVD-G could also act as nucleation sites, but further studies are required to elucidate their role as MoS_2

dx.doi.org/10.1021/nl204562j | *Nano Lett.* 2012, 12, 2784−2791

nucleation centers. For comparison, the precursor adsorption time was also adjusted up to 30 min and 1 h while keeping the carrying gas flow rate at 10 sccm. With the increase of the precursor dose, thicker MoS_2 flakes with a typical thicknesses ranging from ~10 to ~50 nm can be found on the surface of graphene. It was noticed that with a 30 min deposition time produces MoS_2 flakes that are not closely packed (as shown in Figure 2C), but the morphology of the seemingly "empty regions" between the MoS_2 flakes differs dramatically from just CVD-G on Cu foil (no terrace features can be found here). This indicates that the graphene surface is fully covered by a film of MoS_2 and the isolated MoS_2 flakes seen here are on top of the underlying MoS_2 background. For the sample grown with 1 h adsorption, the size of these MoS_2 nanoflakes becomes smaller and the nanoflakes are closely packed (as shown in Figure 2D). A possible evolution path of MoS_2 flakes to continuous MoS_2 film is schematically illustrated in Figure 2E.

The MoS_2/graphene heterostructures were characterized using Raman spectroscopy. The MoS_2/graphene hybrid was first transferred onto SiO_2/Si substrates after etching away the copper foil. The samples display Raman features at 384 $cm^{-1}$and 409 cm^{-1} [51] as shown in the inset of Figure 3, which

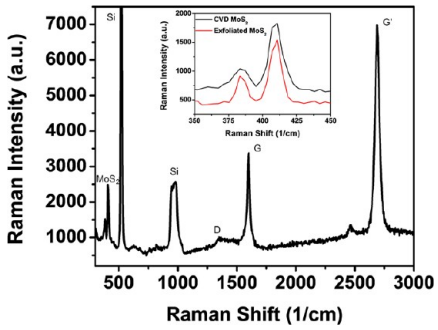

Figure 3. Raman spectra taken from the MoS_2/graphene heterostructure after it is transferred to 300 nm SiO_2/Si substrates. Inset shows the typical Raman signature of CVD synthesized MoS_2 on graphene (spectrum in black) and the one obtained from mechanically exfoliated bulk MoS_2 on SiO_2/Si substrate (spectrum in red).

are characteristic signature of the MoS_2 structure and originate from the E^1_{2g} and A_{1g} Raman modes of MoS_2.[51] The peaks at 520 and ~900 cm^{-1} originates from the Si substrate. The inset spectra in black and red compare the Raman signature of CVD synthesized and bulk MoS_2 crystals (SPI, natural molybdenite mechanically exfoliated onto SiO_2/Si substrates). Consistently with a recent report,[1] the CVD MoS_2 showing a lower relative intensity ratio for E^1_{2g} and A_{1g} compared to the natural MoS_2 crystal. The intensity ratios for E^1_{2g} and A_{1g} are ~0.31 and ~0.45 for the CVD MoS_2 and natural MoS_2, respectively. The difference originates from the fact that the planar vibration mode E^1_{2g} can be affected by the grain distribution and the domain size of the CVD MoS_2.[1,51] In contrast, the peak spacing between E^1_{2g} and A_{1g} for CVD and exfoliated MoS_2 is 25.3 and 25.4 cm^{-1}, respectively. Furthermore, Raman is a useful technique to analyze the quality of graphene.[52] The most direct feature in Raman spectroscopy showing the quality of graphene is the D band at ~1350 cm^{-1}, which is closely related to the defect density in the graphene lattice. The small graphene D band (~1350 cm^{-1}) suggests that under the growth condition used for MoS_2 synthesis, the structure of the graphene was not adversely affected.

To further study the structure and chemical composition of the epitaxial heterostructures we used TEM, EDS, STEM, and XPS characterization techniques. XPS and EELS were applied to characterize the elemental composition of the as-synthesized samples. The atomic ratio of Mo and S obtained from XPS is 1:2.14, which is in a good agreement with the value obtained from EELS . The detailed XPS and EELS measurement are given in the Supporting Information (Figures S1 and S2).

TEM images of the epitaxial MoS_2/graphene heterostructures are shown in Figure 4. The MoS_2/graphene hybrid was transferred to a TEM grid using the method described in the Supporting Information. The MoS_2 flakes show darker contrast compared to the graphene membrane. Figure 4A,B shows typical TEM bright-field images of the MoS_2/graphene hybrid structure with varying densities of MoS_2. Figure 4A presents an isolated hexagonal flake and the inset is the selected area electron diffraction (SAED) pattern taken from this MoS_2 flake. The SAED pattern indicates the single crystalline nature of the hexagonal flake. Figure 4C shows a typical high-resolution TEM (HRTEM) image taken from the edge of a MoS_2 flake. The lattice spacing matches the (100) spacing of MoS_2. The inset shows the EDS spectrum taken from the same region, which confirms the presence of both sulfur and molybdenum in the flake. The full EDS spectrum is given in the Supporting Information (Figure S3).

As mentioned before, with increasing amount of precursor, continuous MoS_2 films form, with loosely packed MoS_2 nanoflakes on top of the film, (see Figure 2C). In order to investigate the crystallinity of the MoS_2 thin film, aberration-corrected STEM high-angle annular dark-field (HAADF)

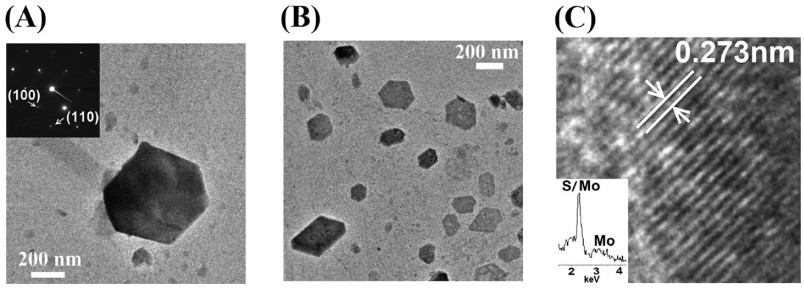

Figure 4. TEM images of the heterostructure of MoS_2 nanoflakes on graphene surface. (A) TEM image of an isolated flake with hexagonal shape. Inset shows the selected area electron diffraction (SAED) pattern from the flake. (B) Low-magnification TEM image of MoS_2 flakes with higher densities (This sample shows a uniform and transparent MoS_2 background (more details are given by the STEM analysis in Figure 6). (C) A typical HRTEM image taken from the edge of a MoS_2 flake. The lattice spacing matches the (100) spacing of MoS_2. Inset shows the EDS spectrum of the MoS_2 flakes.

dx.doi.org/10.1021/nl204562j | Nano Lett. 2012, 12, 2784−2791

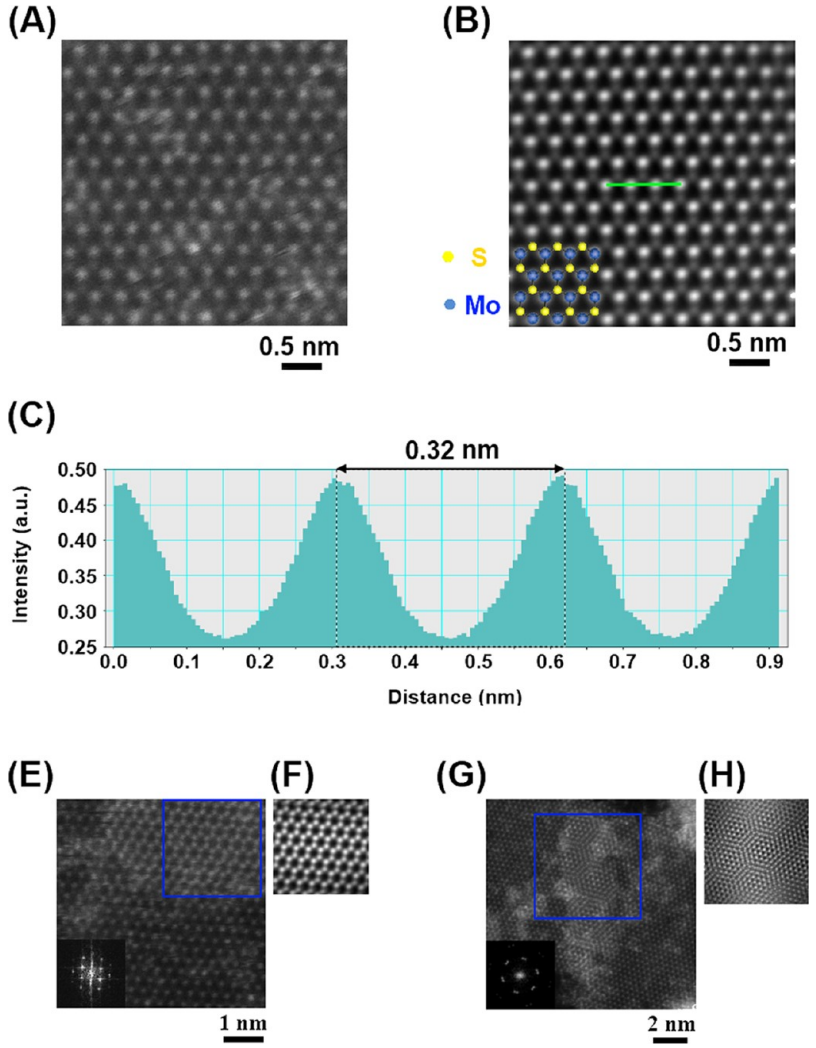

Figure 5. High-resolution STEM-HAADF imaging of the monolayer and few-layer MoS_2 film supported on the graphene membrane. (A) Raw data and (B) FFT-filtered image. The inset shows the overlay of an atomic structure model of monolayer MoS_2 (projection down the *c*-axis). (C) The measured in-plane lattice distance (indicated by the green line in (B)) is 0.32 ± 0.01 nm. (E,G) The high-resolution STEM-HAADF images of a AB stacked and misoriented bilayer MoS_2 (with 8.5° rotation angle) nanodomains respectively; (F,H) the FFT-filtered images of the regions highlighted in E and G, respectively. Insets of panels E and G show the FFT patterns of the highlighted regions.

imaging, also known as *Z*-contrast imaging, was performed. Besides the MoS_2 flakes observed under TEM, single layer and few-layer MoS_2 films can also be clearly observed from the STEM-HAADF images. The result indicates that the MoS_2 synthesis on graphene surface is not a self-limited reaction. Since STEM-HAADF image intensity is atomic number (*Z*) dependent, the Mo and S atomic positions in the monolayer MoS_2 film can be easily identified from the image contrast as shown in Figure 5A. The Mo atoms show much higher contrast than the S atom pairs. The lattice structure of the monolayer MoS_2 is more clearly shown in the Fourier-filtered image in Figure 5B, where direct measurement of the lattice constant is possible. Figure 5C shows an intensity line profile across the filtered image (as marked in Figure 5B), which gives an in-plane lattice constant of 0.32 nm. The STEM results suggest the *c*-axis of the MoS_2 flake is perpendicular to the graphene substrates. Moreover, the HAADF image intensity is also proportional to the number of MoS_2 layers, which provides a feasible way to quantify the number of layers for few-layer MoS_2 films. For the MoS_2 domains with a layer number ≥2, both AB stacking and mis-orientated stacking were observed as shown in Figure 5E,F. For the monolayer MoS_2 in Figure 5A,B, the HAADF images show distinct interatomic image contrast between Mo and S pairs. The AB stacking bilayer region in Figure 5E shows equal intensity for the hexagonal lattice due to the overlapping of the Mo and S pairs in the top and bottom layers. The misorientated bilayer MoS_2 can be distinguished by the Moiré pattern, as shown in Figure 5G,H, and the rotation angle between the two atomic layers can be measured directly from the image's fast Fourier transform (FFT).

The orientation relationship between the monolayer MoS_2 and graphene support was studied by analyzing the FFT images. Here the STEM-HAADF images and bright-field (BF) images were collected simultaneously. While HAADF images provide clear *Z* contrast information for the MoS_2 layer, the BF-STEM images deliver phase contrast from both MoS_2 layer and monolayer graphene film. As shown in Figure 6, the FFT images from the STEM-BF images show diffraction spots from the graphene, even though it is difficult to resolve the graphene lattice directly from the STEM-HAADF or STEM-BF images because of the intrinsic low contrast arising from a single atomic layer. The sharp diffraction spots shown in Figure 6C

dx.doi.org/10.1021/nl204562j | *Nano Lett.* 2012, 12, 2784–2791

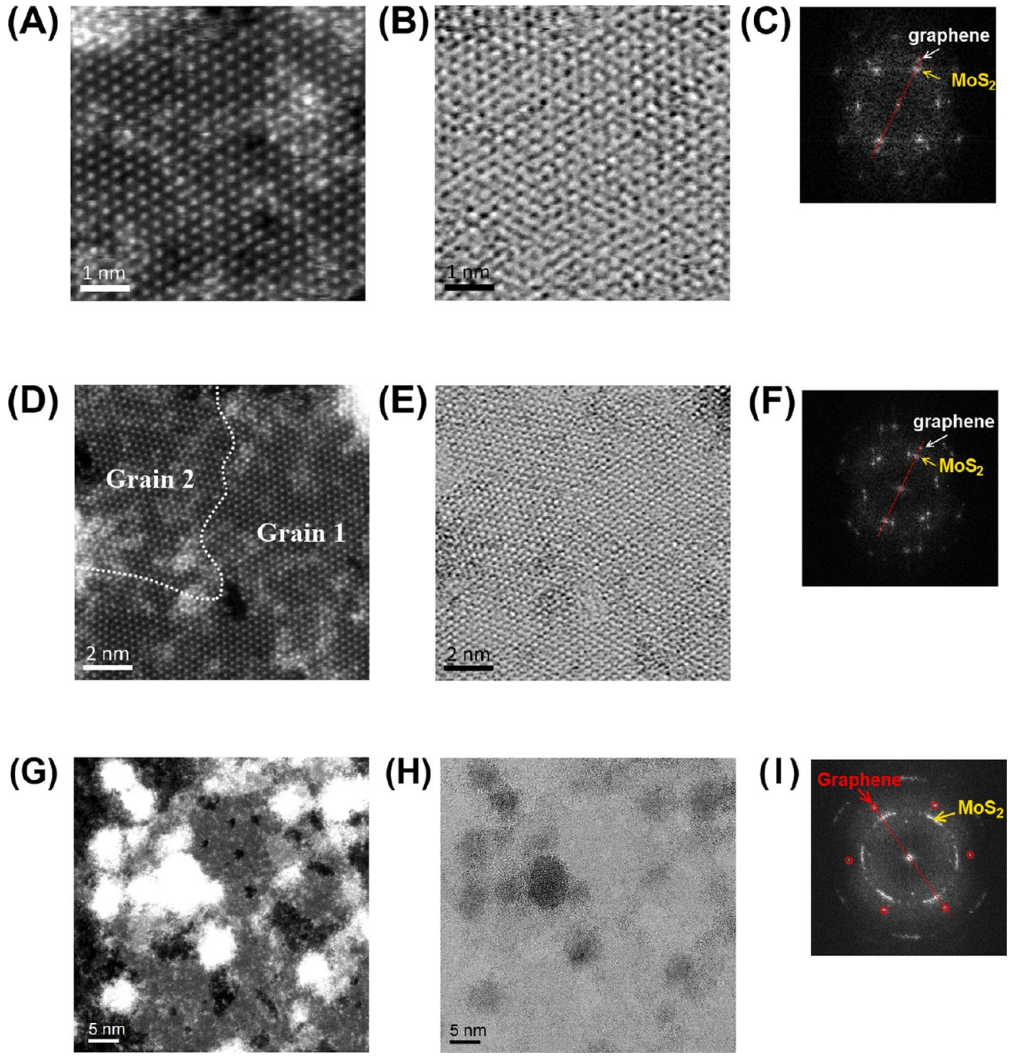

Figure 6. STEM-HAADF images (A,D,G) and STEM-BF images (B,E,H) of the monolayer MoS_2 film supported on the graphene membrane. The white line in panel D roughly shows the grain boundary of MoS_2. Panels C, F, and I are the corresponding FFT patterns from the STEM-BF images in panels B, E, and H, respectively. The arrows indicate the diffraction spots originating from the graphene and the MoS_2 layers. Red dash lines are added to compare both lattices orientation. The brightest particles in panel G are FeO_x residuals induced during transfer process, and one of them generates the sharp spots inside the MoS_2 ring in the FFT pattern.

indicate the single crystal nature of the imaged graphene and MoS_2 domains. More importantly, the MoS_2 domain displays the same orientation as the underneath graphene film, as illustrated by the red dash line in Figure 6C. The result suggests that the MoS_2 grain is epitaxially grown on graphene. However, we notice that the monolayer MoS_2 films are polycrystalline. An example of a grain boundary in the monolayer MoS_2 film is shown in Figure 6D,E. The grain boundary is highlighted by the white line in Figure 6D, and the presence of the two grains can be clearly seen from the images and the corresponding FFT image (Figure 6F). The FFT image further shows that one of the MoS_2 grain (labeled as "Grain 1") is epitaxially grown on the graphene film, while the other MoS_2 grain (labeled as "Grain 2") presents a 12° rotation with respect to the graphene lattice.

To further understand the tendency of epitaxial growth of MoS_2 monolayer on graphene, we look at STEM images from relatively large areas covering multiple MoS_2 grains. A representative example is shown in Figures 6G,H. The corresponding FFT image (Figure 6I) from the BF image shows sharp spots from graphene, indicating that the graphene layer in the imaging area belongs to the same grain. The imaged MoS_2 film generates partial diffracted ring patterns, suggesting the presence of multiple grains with different orientations. However, the partial diffracted rings for MoS_2 shows strong tendency to align with the graphene's diffraction pattern; the diffraction intensity is stronger along the same orientation as the graphene film. Moreover, almost all the diffraction intensity coming from MoS_2 is distributed within a narrow range (from −11 to 18° with respect to the graphene film). This means that a large fraction of the MoS_2 grains is epitaxially grown on the graphene film, and all the MoS_2 grains tend to orient as close as possible to the graphene film.

We observed experimentally that the monolayer MoS_2 film is polycrystalline, and a large fraction of the MoS_2 grains adopt the same orientation as the graphene film. Notice that the lattice spacing for MoS_2 is ∼28% larger than that for graphene, therefore it is likely that the crystal orientation can be incommensurate due to the large strains between layers. However, all the remaining strain is expected to get accommodated in the van der Waals gap. The formation of defects in MoS_2 is probably due to a large number of

dx.doi.org/10.1021/nl204562j | Nano Lett. 2012, 12, 2784−2791

heterogeneous sites (impurities) derived from precursors or grain boundaries (defects) of graphene, where further study would be required.

Our STEM results suggest that the monolayer MoS_2 grains tend to epitaxially grow on graphene, and a misorientation of the MoS_2 monolayer grains with respect to graphene develops gradually. The formation of a continuous partial ring pattern within a narrow angular range, instead of multiple sets of sharp spot patterns, is a strong evidence for the gradual development of mis-orientation from the epitaxial MoS_2 grains. Moreover, the fact that almost no MoS_2 grain shows mis-orientation larger than 18° with respect to the graphene film further confirms that the MoS_2 does not grow randomly on graphene.

In conclusion, we have presented the growth of MoS_2 layered structures on CVD-G through the adsorption and decomposition of a single precursor. Even though there is a large lattice mismatch between the MoS_2 and graphene structure, it was found that graphene can serve as an epitaxial substrate for MoS_2. The remarkable electrical and mechanical properties of graphene make it very suitable both as an electrode and a support substrate/scaffold, whereas the MoS_2 flakes on its surface can serve as catalysis or electron redox centers. Furthermore, our results here also suggest that other hexagonal structured substrates, such as hexagonal boron nitride, can be used as a growth substrate for the MoS_2 layers. h-BN has been shown to be a superior substrate for graphene transistor devices due to the absence of dangling bonds.[7] Potentially the growth of MoS_2 on h-BN may lead to high-performance MoS_2 transistor or optoelectronic devices in the future.

■ ASSOCIATED CONTENT

Supporting Information

Detailed descriptions of the graphene and MoS_2 synthesis method, transfer method of the as-grown MoS_2/graphene hybrids to arbitrary substrates, and the EELS, XPS, and EDS characterization results of the MoS_2/graphene hybrids. This material is available free of charge via the Internet at http://pubs.acs.org.

■ AUTHOR INFORMATION

Corresponding Author

*E-mail: jingkong@mit.edu.

Author Contributions

#These authors contribute equally.

Notes

The authors declare no competing financial interest.

■ ACKNOWLEDGMENTS

This work was supported by the National Science Foundation under Award Number DMR 0845358. W.J.F. acknowledges the support from Interconnect Focus Center (IFC), and K.K.K. acknowledges the support from the Materials, Structure, and Devices (MSD); both are among the five programs in the focus center research program (FCRP), a Semiconductor Research Corporation program. S.M.K. acknowledges the support from National Research Foundation of Korea Grant funded by the Korean Government (NRF-2011-357- C00028). W.Z. acknowledges the support from the National Science Foundation under award No. DMR-0938330; J.C.I. acknowledges support from Oak Ridge National Laboratory's Shared Research Equipment (ShaRE) User Facility, which is sponsored by the Office of Basic Energy Sciences, U.S. Department of Energy. L.J.L. acknowledges the support from Academia Sinica and National Science Council in Taiwan (NSC-99-2112-M-001-021-MY3).

■ REFERENCES

(1) Zhan, Y.; Liu, Z.; Najmaei, S.; Ajayan, P. M.; Lou, J. *Small* **2012**, *8* (7), 966−971.

(2) Liu, K.-K.; Zhang, W.; Lee, Y.-H.; Lin, Y.-C.; Chang, M.-T.; Su, C.-Y.; Chang, C.-S.; Li, H.; Shi, Y.; Zhang, H.; Lai, C.-S.; Li, L.-J. *Nano Lett.* **2012**, *12* (3), 1538−1544.

(3) Geim, A. K.; Novoselov, K. S. *Nat. Mater.* **2007**, *6* (3), 183−191.

(4) Novoselov, K. S.; Geim, A. K.; Morozov, S. V.; Jiang, D.; Katsnelson, M. I.; Grigorieva, I. V.; Dubonos, S. V.; Firsov, A. A. *Nature* **2005**, *438* (7065), 197−200.

(5) Novoselov, K. S.; Geim, A. K.; Morozov, S. V.; Jiang, D.; Zhang, Y.; Dubonos, S. V.; Grigorieva, I. V.; Firsov, A. A. *Science* **2004**, *306* (5696), 666−669.

(6) Kubota, Y.; Watanabe, K.; Tsuda, O.; Taniguchi, T. *Science* **2007**, *317* (5840), 932−934.

(7) Dean, C. R.; Young, A. F.; Meric, I; Lee, C; Wang, L; Sorgenfrei, S; Watanabe, K; Taniguchi, T; Kim, P; Shepard, K. L.; Hone, J. *Nat. Nanotechnol.* **2010**, *5* (10), 722−726.

(8) Zhang, Y.; Tan, Y.-W.; Stormer, H. L.; Kim, P. *Nature* **2005**, *438* (7065), 201−204.

(9) Decker, R. g.; Wang, Y.; Brar, V. W.; Regan, W.; Tsai, H.-Z.; Wu, Q.; Gannett, W.; Zettl, A.; Crommie, M. F. *Nano Lett.* **2011**, *11* (6), 2291−2295.

(10) Zeng, H.; Zhi, C.; Zhang, Z.; Wei, X.; Wang, X.; Guo, W.; Bando, Y.; Golberg, D. *Nano Lett.* **2010**, *10* (12), 5049−5055.

(11) Radisavljevic, B; Radenovic, A; Brivio, J; Giacometti, V; Kis, A. *Nat. Nanotechnol.* **2011**, *6* (3), 147−150.

(12) Eda, G.; Yamaguchi, H.; Voiry, D.; Fujita, T.; Chen, M.; Chhowalla, M. *Nano Lett.* **2011**, *11* (12), 5111−5116.

(13) Splendiani, A.; Sun, L.; Zhang, Y.; Li, T.; Kim, J.; Chim, C.-Y.; Galli, G.; Wang, F. *Nano Lett.* **2010**, *10* (4), 1271−1275.

(14) Brivio, J.; Alexander, D. T. L.; Kis, A. *Nano Lett.* **2011**, *11* (12), 5148−5153.

(15) Mak, K. F.; Lee, C.; Hone, J.; Shan, J.; Heinz, T. F. *Phys. Rev. Lett.* **2010**, *105* (13), 136805.

(16) Coleman, J. N.; Lotya, M.; O'Neill, A.; Bergin, S. D.; King, P. J.; Khan, U.; Young, K.; Gaucher, A.; De, S.; Smith, R. J.; Shvets, I. V.; Arora, S. K.; Stanton, G.; Kim, H.-Y.; Lee, K.; Kim, G. T.; Duesberg, G. S.; Hallam, T.; Boland, J. J.; Wang, J. J.; Donegan, J. F.; Grunlan, J. C.; Moriarty, G.; Shmeliov, A.; Nicholls, R. J.; Perkins, J. M.; Grieveson, E. M.; Theuwissen, K.; McComb, D. W.; Nellist, P. D.; Nicolosi, V. *Science* **2011**, *331* (6017), 568−571.

(17) Gordon, R. A.; Yang, D.; Crozier, E. D.; Jiang, D. T.; Frindt, R. F. *Phys. Rev. B* **2002**, *65* (12), 125407.

(18) Yin, Z.; Li, H.; Li, H.; Jiang, L.; Shi, Y.; Sun, Y.; Lu, G.; Zhang, Q.; Chen, X.; Zhang, H. *ACS Nano* **2012**, *6* (1), 74−80.

(19) Cai, G. M.; Jian, J. K.; Chen, X. L.; Lei, M.; Wang, W. Y. *Appl. Phys. A* **2007**, *89* (3), 783−788.

(20) Viršek, M.; Krause, M.; Kolitsch, A.; Mrzel, A.; Iskra, I.; Škapin, S. o. D.; Remškar, M. *J. Phys. Chem. C* **2010**, *114* (14), 6458−6463.

(21) Kim, D.; Sun, D.; Lu, W.; Cheng, Z.; Zhu, Y.; Le, D.; Rahman, T. S.; Bartels, L. *Langmuir* **2011**, *27* (18), 11650−11653.

(22) Lee, Y.-H.; Zhang, X.-Q.; Zhang, W.; Chang, M.-T.; Lin, C.-T.; Chang, K.-D.; Yu, Y.-C.; Wang, J. T.-W.; Chang, C.-S.; Li, L.-J.; Lin, T.-W. *Adv. Mater.* **2012**, *24* (17), 2320−2325.

(23) Diemann, E.; Müller, A.; Aymonino, P. J. *Z. Anorg. Allg. Chem.* **1981**, *479* (8), 191−198.

(24) Prasad, T. P.; Diemann, E.; Müller, A. *J. Inorg. Nucl. Chem.* **1973**, *35* (6), 1895−1904.

(25) Song, X. C.; Zhao, Y.; Zheng, Y. F.; Yang, E. *Adv. Eng. Mater.* **2007**, *9* (1−2), 96−98.

(26) Piña, C.; Bosch, P.; Acosta, D.; Barreto, J.; Vazquez, A.; Camarillo, E. *J. Cryst. Growth* **1989**, *96* (3), 685−690.

(27) Remskar, M.; Mrzel, A.; Skraba, Z.; Jesih, A.; Ceh, M.; Demsar, J.; Stadelmann, P.; Levy, F.; Mihailovic, D. *Science* **2001**, *292* (5516), 479−481.

(28) Ma, L.; Chen, W.-X.; Li, H.; Zheng, Y.-F.; Xu, Z.-D. *Mater. Lett.* **2008**, *62* (6−7), 797−799.
(29) Peng, Y. Y.; Meng, Z. Y.; Zhong, C.; Lu, J.; Yu, W. C.; Jia, Y. B.; Qian, Y. T. *Chem. Lett.* **2001**, No. 8, 772−773.
(30) Zou, T. Z.; Tu, J. P.; Huang, H. D.; Lai, D. M.; Zhang, L. L.; He, D. N. *Adv. Eng. Mater.* **2006**, *8* (4), 289−293.
(31) Kim, K. S.; Zhao, Y.; Jang, H.; Lee, S. Y.; Kim, J. M.; Kim, K. S.; Ahn, J.-H.; Kim, P.; Choi, J.-Y.; Hong, B. H. *Nature* **2009**, *457* (7230), 706−710.
(32) Reina, A.; Jia, X.; Ho, J.; Nezich, D.; Son, H.; Bulovic, V.; Dresselhaus, M. S.; Kong, J. *Nano Lett.* **2008**, *9* (1), 30−35.
(33) Li, X.; Cai, W.; An, J.; Kim, S.; Nah, J.; Yang, D.; Piner, R.; Velamakanni, A.; Jung, I.; Tutuc, E.; Banerjee, S. K.; Colombo, L.; Ruoff, R. S. *Science* **2009**, *324* (5932), 1312−1314.
(34) Shi, Y.; Hamsen, C.; Jia, X.; Kim, K. K.; Reina, A.; Hofmann, M.; Hsu, A. L.; Zhang, K.; Li, H.; Juang, Z.-Y.; Dresselhaus, M. S.; Li, L.-J.; Kong, J. *Nano Lett.* **2010**, *10* (10), 4134−4139.
(35) Liu, Z.; Song, L.; Zhao, S.; Huang, J.; Ma, L.; Zhang, J.; Lou, J.; Ajayan, P. M. *Nano Lett.* **2011**, *11* (5), 2032−2037.
(36) Kim, K. K.; Hsu, A.; Jia, X.; Kim, S. M.; Shi, Y.; Hofmann, M.; Nezich, D.; Rodriguez-Nieva, J. F.; Dresselhaus, M. S.; Palacios, T.; Kong, J. *Nano Lett.* **2012**, *1* (12), 161−166.
(37) Li, Y.; Wang, H.; Xie, L.; Liang, Y.; Hong, G.; Dai, H. *J. Am. Chem. Soc.* **2011**, *133* (19), 7296−7299.
(38) Yan, K.; Peng, H.; Zhou, Y.; Li, H.; Liu, Z. *Nano Lett.* **2011**, *11* (3), 1106−1110.
(39) Dang, W.; Peng, H.; Li, H.; Wang, P.; Liu, Z. *Nano Lett.* **2010**, *10* (8), 2870−2876.
(40) Koma, A.; Sunouchi, K.; Miyajima, T. *J. Vac. Sci. Technol., B* **1985**, *3* (2), 724−724.
(41) Koma, A. *Thin Solid Films* **1992**, *216* (1), 72−76.
(42) Ma, Y.; Dai, Y.; Guo, M.; Niu, C.; Huang, B. *Nanoscale* **2011**, *3* (9), 3883−3887.
(43) Zong, X.; Wu, G.; Yan, H.; Ma, G.; Shi, J.; Wen, F.; Wang, L.; Li, C. *J. Phys. Chem. C* **2010**, *114* (4), 1963−1968.
(44) Zong, X.; Yan, H.; Wu, G.; Ma, G.; Wen, F.; Wang, L.; Li, C. *J. Am. Chem. Soc.* **2008**, *130* (23), 7176−7177.
(45) Li, H.; Yin, Z.; He, Q.; Li, H.; Huang, X.; Lu, G.; Fam, D. W. H.; Tok, A. I. Y.; Zhang, Q.; Zhang, H. *Small* **2012**, *8* (1), 63−67.
(46) Chang, K.; Chen, W. *ACS Nano* **2011**, *5* (6), 4720−4728.
(47) Xiao, J.; Choi, D.; Cosimbescu, L.; Koech, P.; Liu, J.; Lemmon, J. P. *Chem. Mater.* **2010**, *22* (16), 4522−4524.
(48) Hwang, H.; Kim, H.; Cho, J. *Nano Lett.* **2011**, *11* (11), 4826−4830.
(49) Ki Kang, K.; Alfonso, R.; Yumeng, S.; Hyesung, P.; Lain-Jong, L.; Young Hee, L.; Jing, K. *Nanotechnology* **2010**, *21* (28), 285205.
(50) An, J.; Voelkl, E.; Suk, J. W.; Li, X.; Magnuson, C. W.; Fu, L.; Tiemeijer, P.; Bischoff, M.; Freitag, B.; Popova, E.; Ruoff, R. S. *ACS Nano* **2011**, *5* (4), 2433−2439.
(51) Lee, C.; Yan, H.; Brus, L. E.; Heinz, T. F.; Hone, J.; Ryu, S. *ACS Nano* **2010**, *4* (5), 2695−2700.
(52) Dresselhaus, M. S.; Jorio, A.; Hofmann, M.; Dresselhaus, G.; Saito, R. *Nano Lett.* **2010**, *10* (3), 751−758.